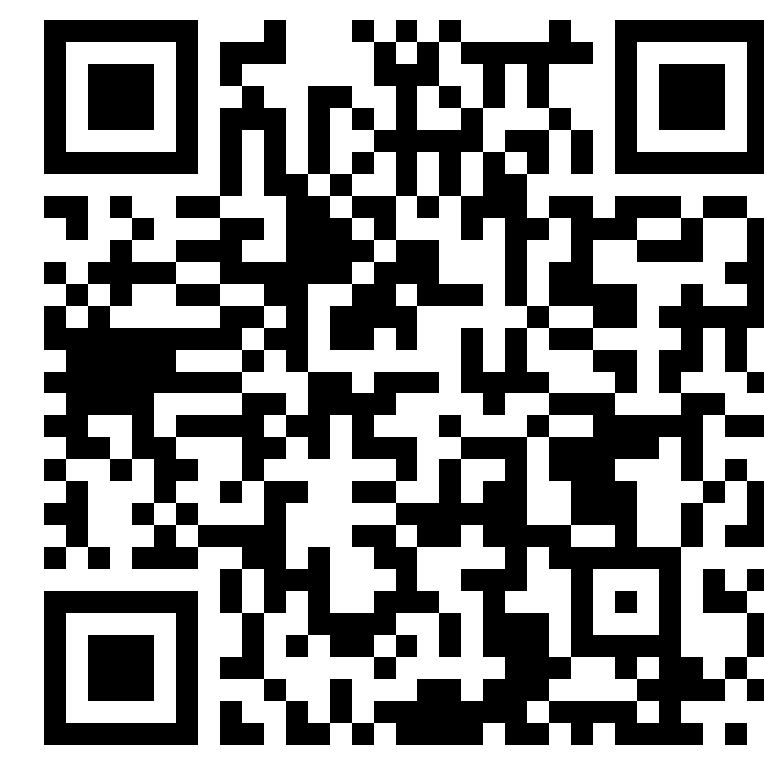


# The Jovian ionospheric conductivity derived from a broadband precipitated electron distribution

G. Sicorello<sup>1</sup>, B. Bonfond<sup>1</sup>, J.-C. Gérard<sup>1</sup>, D. Grodent<sup>1</sup>, L. Gkouvelis<sup>2</sup>, G.R. Gladstone<sup>3,4</sup> and A. Salveter<sup>5</sup>

<sup>1</sup>ULiège (Belgium), <sup>2</sup>LMU München (Germany), <sup>3</sup>SwRI (Texas), <sup>4</sup>UTSA (Texas), <sup>5</sup>UoC (Germany)

Contact: guillaume.sicorello@uliege.be



## In a nutshell

- The conductivity at Jupiter is almost always computed assuming a simple mono-energetic auroral electron precipitation at high latitudes.
- The effect of a more realistic broadband electron distribution on the conductivity is investigated.
- Our model shows that mono-energetic distributions either overestimate (up to 1.6-fold) or underestimate (up to 10-fold) the conductance, depending on the mean energy of the precipitating electrons.

## 1. Introduction

The **Pedersen ionospheric conductivity and conductance** at Jupiter are key elements when considering the exchange of momentum and energy between the ionosphere and the magnetosphere.

Most models assume a **mono-energetic** distribution to represent the electron flux (e.g. Gérard *et al.*, 2020). However, based on the recent findings from the Juno spacecraft, it appears that the impinging electron distribution is best approximated with a **broadband** distribution (e.g. Mauk *et al.*, 2017; Salveter *et al.*, 2022). **What are the effects of such a distribution on the conductivity/conductance?**

## 2. Ionospheric model

The ionospheric model presented in Gérard *et al.* (2020) is adopted:

- Altitude distributions of **H**, **H<sub>2</sub>** and **CH<sub>4</sub>** taken from Grodent *et al.* (2001) model.
- Above the homopause, conductivity mainly driven by the **H<sub>3</sub><sup>+</sup> ion**:



- Close to and below the homopause, rapid reaction of CH<sub>4</sub> with H<sub>3</sub><sup>+</sup> produces **hydrocarbon ions** responsible for the conductivity. **CH<sub>5</sub><sup>+</sup>** is considered as the main hydrocarbon product (Wang *et al.*, 2021):



- H<sub>2</sub><sup>+</sup> profile computed using the formulation given by Hiraki & Tao (2008).

## 3. Conductivity $\sigma_P$ and conductance $\Sigma_P$

$$\sigma_P = e^2 n_e \left[ \frac{\nu_{en}}{m_e(\nu_{en}^2 + \omega_e^2)} + \sum_i \frac{\nu_{in}}{m_i(\nu_{in}^2 + \omega_i^2)} \right], \quad \Sigma_P = \int \sigma_P dz.$$

- $e$ : electron charge.
- $\nu_{en}(\nu_{in})$ : electron (ion)-neutral collision frequency.
- $m_e(m_i)$ : electron (ion) mass.
- $\omega_e(\omega_i)$ : electron (ion) gyrofrequency.
- $z$ : altitude.

## 4. Kappa distribution

The kappa function  $f$  is chosen to model the broadband shape of the electron energy distribution (Coumans *et al.*, 2002). It is defined by the **total energy flux**  $Q_0$  (unit: mW.m<sup>-2</sup>), the **mean energy**  $\langle E \rangle$  (unit: keV) and an additional parameter  $\kappa$  describing the high energy tail of the distribution:

$$f(E) = \frac{4Q_0}{\pi} \frac{\kappa(\kappa-1)}{(\kappa-2)^2} \frac{E}{\langle E \rangle} \frac{\langle E \rangle^{\kappa-1}}{\left(\frac{2E}{\kappa-2} + \langle E \rangle\right)^{\kappa+1}}$$

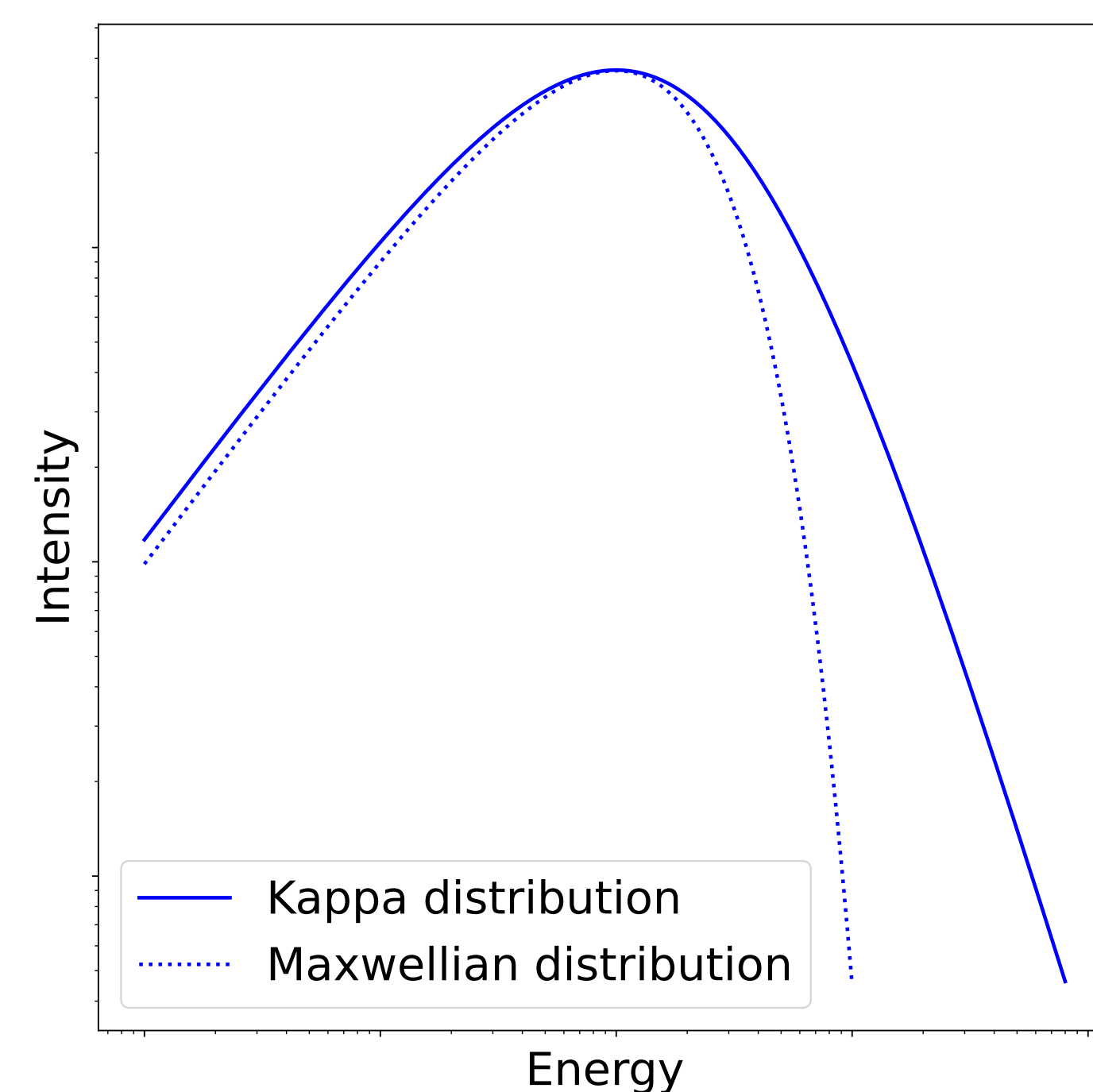
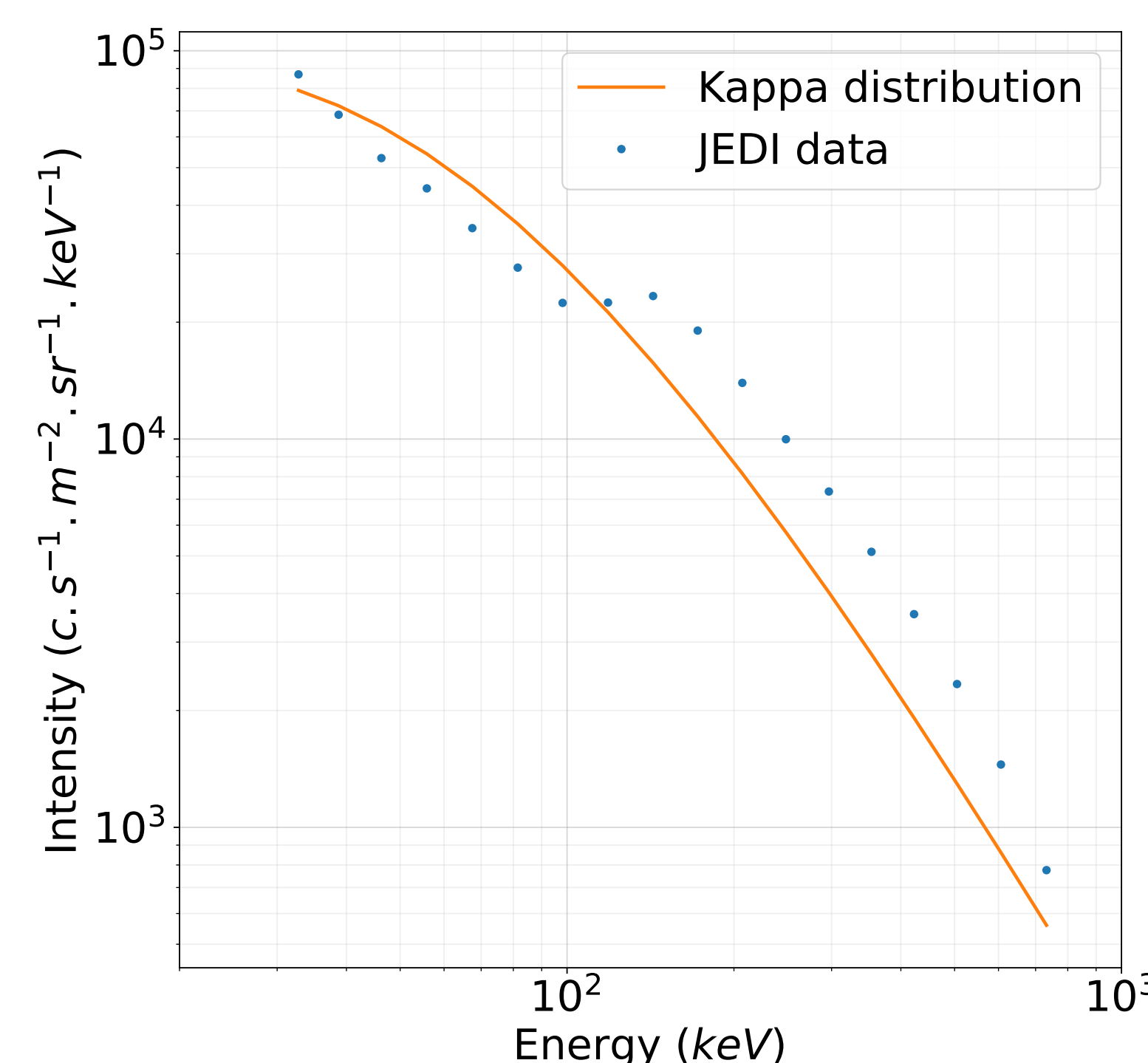


**Fig. 1:** Representation of a **maxwellian and a kappa distributions** with the same intensity at the energy peak. At low energy, both distributions are similar. However, the kappa distribution has a high-energy tail that decreases as a power law.

**Fig. 2:** Kappa distribution displayed over electron distribution measurements. The data points represent the median values of the intensities measured by Juno/JEDI over the main emission during perijoves 1 to 20. With a value of  $\kappa = 2.5$ , the kappa function appears to be a **good representation** of the electron energy distribution.



## 5. Results

The curve on Fig. 4 is explained by the existence of a conductance maximum around the mean energy value  $E_{\text{max}}=30$  keV (Gérard *et al.*, 2020):

- (1)-(3): Mean energy away from  $E_{\text{max}} \rightarrow$  **enhanced broadband conductance**.
- (2): Mean energy close to  $E_{\text{max}} \rightarrow$  **enhanced mono-energetic conductance**.

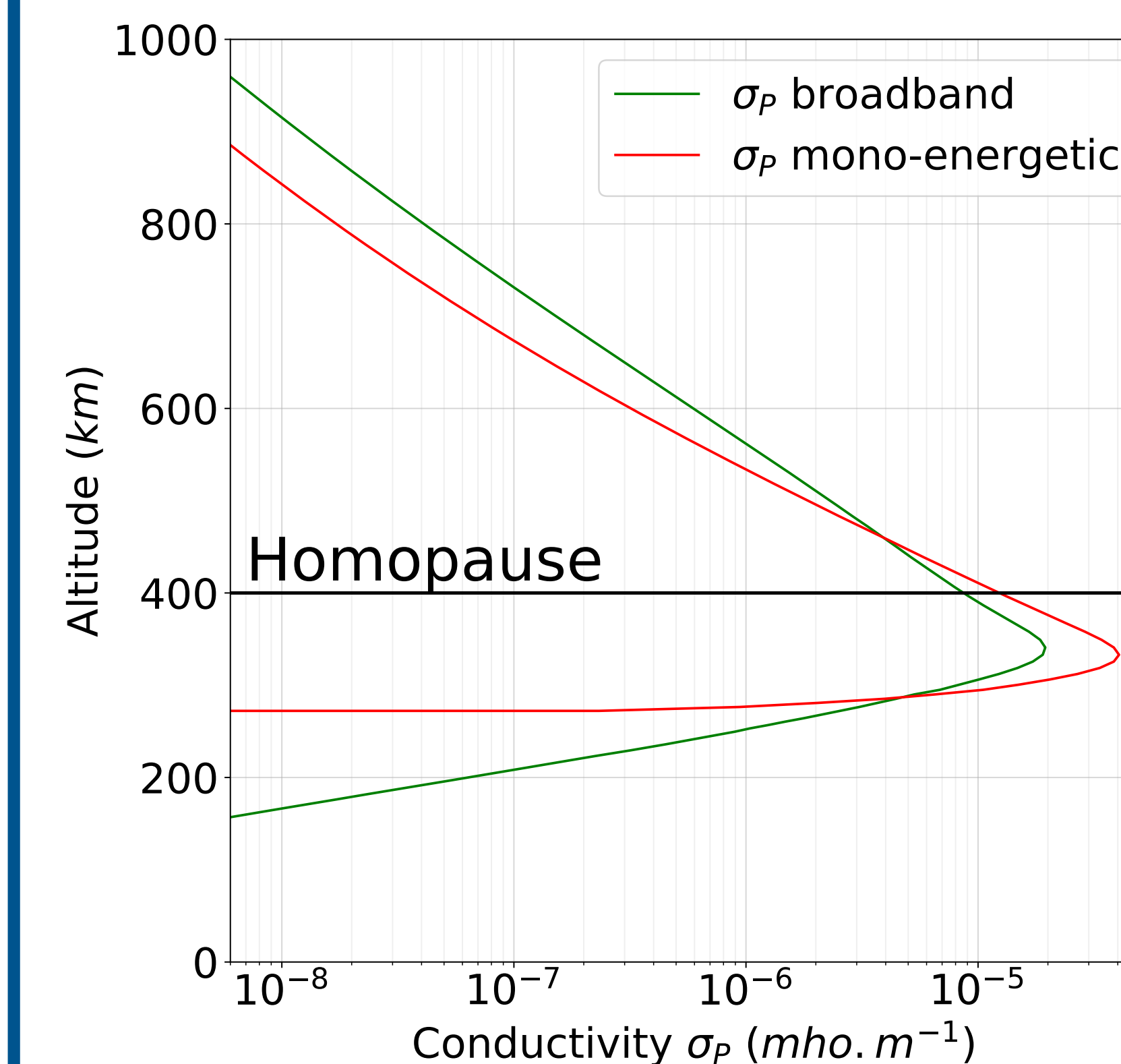


**Fig. 3:** Comparison between **mono-energetic and broadband vertical profile conductivities** ( $Q_0=100$  mW.m<sup>-2</sup>,  $\langle E \rangle=40$  keV). Understandably, the broadband distribution leads to a broader vertical distribution.

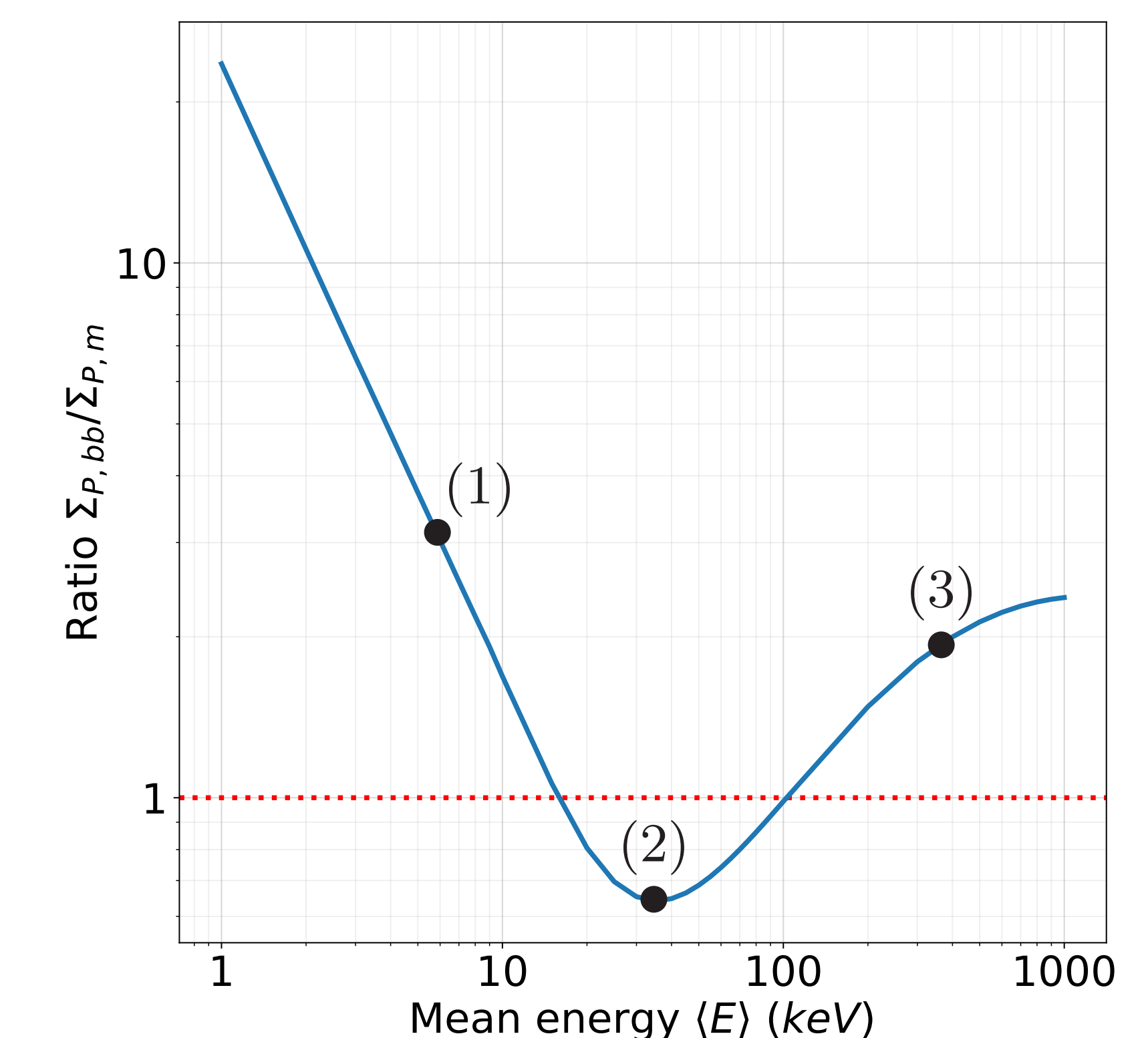


**Fig. 4:** Ratio between mono-energetic (m) and broadband (bb) conductances as a function of the mean electron energy ( $Q_0=100$  mW.m<sup>-2</sup>). Even if the ratio greatly depends on the mean energy, it is **almost never equal to 1**.

## 6. Conclusions

- Compared to a broadband distribution, the conductance deduced from a mono-energetic distribution is either **overestimated by a factor 1.6 in the 15-100 keV range** or **underestimated by a factor of 10 or more outside this range**.
- The next step of this work will be to update the models and conductance maps to better fit the Juno JADE and JEDI observations.

## 7. References

- Coumans, V., Gérard, J.-C., Hubert, B., *et al.* 2002. *J. Geophys. Res. Space Phys.*, **107**(A11), SIA5-1–SIA5-12.
- Grodent, D., Waite Jr., J.H., & Gérard, J.-C. 2001. *J. Geophys. Res. Space Phys.*, **106**(A7), 12933–12952.
- Gérard, J.-C., Gkouvelis, L., Bonfond, B., *et al.* 2020. *J. Geophys. Res. Space Phys.*, **125**(8), e2020JA028142.
- Hiraki, Y., & Tao, C. 2008. *Ann. Geophys.*, **26**(1), 77–86.
- Mauk, B., Haggerty, D., Paranicas, C., *et al.* 2017. *Nature*, **549**(7670), 66–69.
- Salveter, A., Saur, J., Clark, G., *et al.* 2022. *J. Geophys. Res. Space Phys.*, **127**(8), e2021JA030224.
- Wang, Y., Blanc, M., Louis, C., *et al.* 2021. *J. Geophys. Res. Space Phys.*, **126**(9), e2021JA029469.